

Mid-Infrared ultra-high-Q resonators based on fluoride crystalline materials

C. Lecaplain,^{1,*} C. Javerzac-Galy,^{1,*} M. L. Gorodetsky,^{2,3} and T. J. Kippenberg^{1,†}

¹*École Polytechnique Fédérale de Lausanne (EPFL), CH-1015, Lausanne, Switzerland*

²*Russian Quantum Center, Skolkovo 143025, Russia*

³*Faculty of Physics, M. V. Lomonosov Moscow State University, Moscow 119991, Russia*

Decades ago, the losses of glasses in the near-infrared (near-IR) were investigated in views of developments for optical telecommunications [1]. Today, properties in the mid-infrared (mid-IR) are of interest for molecular spectroscopy applications [2–4]. In particular, high-sensitivity spectroscopic techniques based on high-finesse mid-IR cavities hold high promise for medical applications [4–6]. Due to exceptional purity and low losses, whispering gallery mode microresonators based on polished alkaline earth metal fluoride crystals (i.e the XF_2 family, where $\text{X} = \text{Ca}, \text{Mg}, \text{Ba}, \text{Sr}, \dots$) have attained ultra-high quality (Q) factor resonances ($Q > 10^8$) in the near-IR and visible spectral ranges [7]. Here we report for the first time ultra-high Q factors in the mid-IR using crystalline microresonators. Using an uncoated chalcogenide (ChG) tapered fiber, light from a continuous wave quantum cascade laser (QCL) is efficiently coupled to several crystalline microresonators at $4.4 \mu\text{m}$ wavelength. We measure the optical Q factor of fluoride crystals in the mid-IR using cavity ringdown technique. We observe that MgF_2 microresonators feature quality factors that are very close to the fundamental absorption limit, as caused by the crystal's multiphonon absorption ($Q \sim 10^7$), in contrast to near-IR measurements far away from these fundamental limits. Due to lower multiphonon absorption in BaF_2 and SrF_2 , we show that ultra-high quality factors of $Q \geq 1.4 \times 10^8$ can be reached at $4.4 \mu\text{m}$. This corresponds to an optical finesse of $\mathcal{F} > 4 \cdot 10^4$, the highest value achieved for any type of mid-IR resonator to date, and a more than 10-fold improvement over the state-of-the-art [8–10]. Such compact ultra-high Q crystalline microresonators provide a route for narrow-linewidth frequency-stabilized QCL [11] or mid-IR Kerr comb generation.

I. INTRODUCTION

The mid-infrared (mid-IR) spectral window ($\lambda \sim 2.5\text{--}20 \mu\text{m}$) is a highly useful range for spectroscopy, chemical and biological sensing, materials science and industry as it includes strong rotational-vibrational absorption lines of many molecules as well as two atmospheric transmission windows of $3\text{--}5 \mu\text{m}$ and $8\text{--}13 \mu\text{m}$. In this band, the absorption strengths of molecular transitions are typically 10 to 1000 times greater than those in the visible or near-infrared (near-IR), offering the potential to identify the presence of substances with extremely high sensitivity and selectivity, as required in trace-gas detection [3, 6, 10], breath analysis [2, 4] and pharmaceutical process monitoring. The invention of the quantum cascade laser (QCL) [12] was a scientific and technological milestone in the development of mid-IR laser sources. Today, continuous wave QCL operate at room temperature, offer high output power (Watts) and are a commercial technology [13]. These features lead to their wide adoption for spectroscopic applications in the mid-IR region. However their free running linewidth is subject to undesired noise that makes their frequency stabilization challenging [14]. High finesse optical cavities have the potential for substantial reduction of

laser noise [15, 16] and have been recently investigated [11].

The exploration of ultra-high quality (Q) cavities in the mid-IR is a relatively new area driven by the development of QCL frequency stabilization [11], ultra-sensitive molecular sensors [17], cavity-based spectroscopy [2, 18] and optical frequency combs [19]. ZBLAN [20] and chalcogenide glasses [21] resonators appear as promising for mid-IR wavelengths. Moreover, the silicon platform [22] have enabled the fabrication of mid-IR microresonators at $\lambda \sim 5 \mu\text{m}$. To date, Q factors of 10^5 are already achieved in silicon-on-sapphire [23] and chalcogenide glass-on-silicon [24], whereas Q factors of 10^4 are obtained in silicon-on-calcium fluoride [25]. Yet to date, achieving ultra-high Q factors in the mid-IR (or correspondingly high optical finesse) is an outstanding challenge. In the near-IR, high finesse is achieved using Fabry-Pérot cavities based on supermirrors [26] or using microcavities based on WGM. Interference coatings based on substrate-transferred single-crystal multilayers show the potential for ≤ 100 ppm of optical losses in the mid-infrared (potentially out to $7 \mu\text{m}$) [27].

Owing to low material losses, crystalline whispering gallery mode (WGM) microresonators [7] exhibit the highest Q factors in the near-IR and visible spectral ranges (along with the highest reported optical finesse of $\mathcal{F} \sim 10^7$ [28]). Ultra-high Q factors ($> 10^8$) are routinely obtained in magnesium fluoride (MgF_2) and calcium fluoride (CaF_2) [29, 30] and can be as high as

* These authors contributed equally to this work

† tobias.kippenberg@epfl.ch

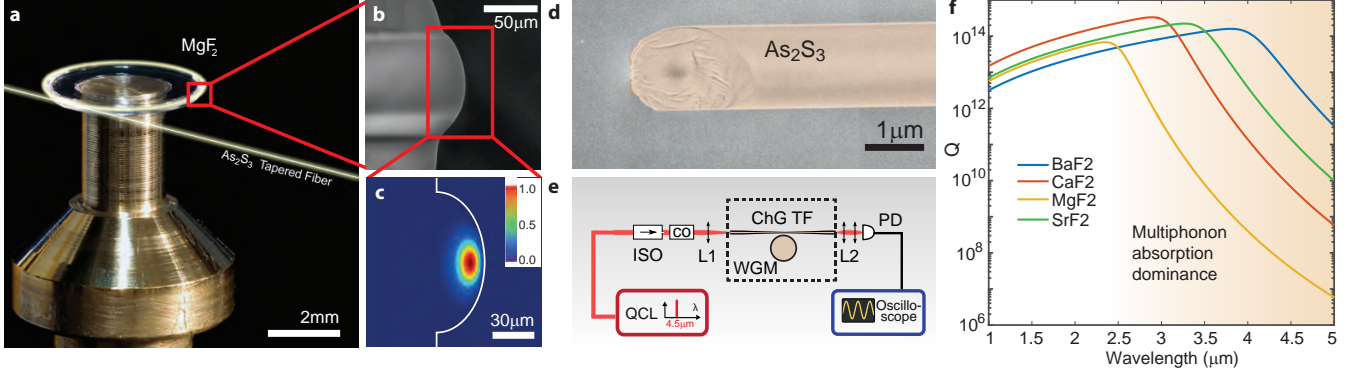


FIG. 1. **Alkaline earth metal fluoride based crystalline microresonators, chalcogenide tapered fiber technology and Q factor dependence of fluoride materials.** **a** Magnesium fluoride (MgF_2) crystalline microresonator with a diameter of ~ 5 mm. Whispering Gallery Modes (WGMs) of the microresonator are excited via evanescent coupling using a chalcogenide i.e. ChG (As_2S_3) tapered fiber. **b** Scanning electron microscope (SEM) image of the MgF_2 protrusion. Its radius of curvature, which confines the mode in the azimuthal direction, is ~ 50 μm . **c** Finite element model simulations of the optical intensity profile of the fundamental WGM at $\lambda = 4.5$ μm . **d** SEM image of the waist of a ChG tapered fiber with subwavelength diameter of 1.2 μm . **e** Experimental setup composed of a WGM microresonator pumped by a quantum cascade laser (QCL) evanescently coupled through a chalcogenide tapered fiber (ChG TF), followed by an oscilloscope to record the transmission. An optical isolator (ISO) protects the pump laser from Fresnel reflection ($\sim 14\%$) at the cleaved fiber ends. Mid-IR free space control optics (CO), including waveplates, neutral densities and a mid-IR electro-optic modulator. L1, L2 are lenses for free space coupling into the ChG TF. PD, photodetector. Tapered fiber and microresonator are kept under a dry and inert atmosphere to preserve from degradation. **f** Quality factor dependence of different crystals with respect to the wavelength. For mid-IR wavelengths, multiphonon absorption competes with Rayleigh scattering and strongly impacts the Q factor.

10^{11} in CaF_2 [28]. Recently, soft fluoride crystals such as barium fluoride (BaF_2) and strontium fluoride (SrF_2) have equally demonstrated ultra-high Q in the near-IR [31, 32]. Such ultra-high Q factors have allowed to observe Kerr comb generation [7] as well as temporal dissipative soliton formation [33, 34] at low (mW) power levels, and enabled low phase noise microwave generation [7] as well as lasers with ultra narrow-linewidth [16]. However, little is known what concerns the actual properties of crystalline microresonators in the mid-IR. Using QCL, recent work have reported Q factors of $\sim 10^7$ at 4.5 μm in MgF_2 [35, 36], CaF_2 [35, 36] and BaF_2 microresonators [36], therefore being more than two orders of magnitude lower than the near-IR values.

Here we study systematically the optical Q factors of four crystalline materials transparent in the mid-IR window of the alkaline earth metal fluoride XF_2 family (where $\text{X} = \text{Ca}, \text{Mg}, \text{Ba}, \text{Sr}$). Note that other combinations such as $\text{X} = \text{Be}, \text{Ra}$ are water soluble or toxic and therefore not suitable. To study the Q factors in the mid-IR we developed an efficient coupling technique based on an optical tapered fiber made out of chalcogenide (ChG) glass. It enables that light from a QCL can be evanescently coupled to a crystalline microresonator via a ChG uncoated tapered fiber. We show that critical coupling [37] is achieved with high ideality [38], necessary for faithful Q factor measurements, and extending this technique for the first time to the mid-IR. We measured a critical factor of $Q_c \sim 1 \times 10^7$ of the MgF_2 microresonator, a value close to the theoretical limit of multiphonon absorption at this wavelength [36]. Using a cavity ringdown method,

we demonstrate for the first time ultra-high Q ($> 10^8$) mid-IR resonances in BaF_2 and SrF_2 microresonators. They feature ultra-high optical quality factors of $Q \geq 1.4 \times 10^8$ at 4.4 μm (more than a ten-fold improvement compared to previous results), exhibiting the highest observed finesse of $\mathcal{F} \sim 4 \times 10^4$ for any cavity in the mid-IR so far. Indeed the finesse of a cavity $\mathcal{F} = \frac{\Delta\lambda}{\delta\lambda}$ relates its free spectral range $\Delta\lambda$ to the linewidth of its resonances $\delta\lambda$ and determines the resolution of many optical measurement methods. These losses, when expressed as mirror losses in an equivalent Fabry-Pérot cavity correspond to a mirror loss of 150 ppm at 4.4 micron.

II. MID-IR CRYSTALLINE MICRORESONATORS PROPERTIES AND FABRICATION

We are interested in crystalline materials whose transparency window includes the region of $3\text{--}5$ μm , a range where QCL are commercially available. We studied four different crystalline materials such as MgF_2 , CaF_2 , BaF_2 and SrF_2 , which are available commercially with high purity (and used e.g. for deep UV lenses). These crystals feature ultra-high Q in the near-IR [29–32] and anomalous group velocity dispersion in the mid-IR, a requirement for Kerr comb and (bright) temporal soliton formation based on the Kerr nonlinearity. However, the theoretically predicted limiting loss mechanism of the Q factor in the mid-IR results from multiphonon absorption

processes [1, 39, 40], involving the coupling of the incident light with fundamental molecular vibrational modes of the material, a loss mechanism not observed so far in the near-IR in such crystals. Usually this reduces the mid-IR cut-off wavelength to a much shorter value than that of the transparency window's maximum wavelength. In the multiphonon-dominated regime the attenuation is given by $\alpha = Ae^{-\beta/\lambda}$ and largely surpasses any Rayleigh scattering contribution proportional to $\frac{B}{\lambda^4}$, where A , β and B are materials properties [1]. Therefore the Q factor limit is given by $Q = \frac{2\pi n}{\alpha\lambda}$ where n is the refractive index and λ the wavelength. Figure 1(f) presents the dependence of the Q factor with respect to the wavelength for alkali earth metal fluoride crystalline materials [41]. It reveals that even though a material displays low Rayleigh scattering and ultra-high Q in the near-IR, it will be subject to multiphonon absorption in the mid-IR that increases by ~ 2 -6 orders of magnitude at $4.5 \mu\text{m}$ compared to $1.5 \mu\text{m}$ for these crystal families. Based on theoretical considerations alone, BaF_2 and SrF_2 seem ideal candidates to achieve ultra-high Q in the mid-IR in comparison to MgF_2 due to lower multiphonon absorption. Though there has been considerable interest in highly-transparent infrared materials for the last decades, only spectrophotometric measurements were carried out to study absorption due to technical limitations of using microresonators in the mid-IR [1, 39, 40]. We emphasize that conventional methods (e.g. Fourier transform infrared spectroscopy) to investigate loss are not suitable to probe the losses at the level of ppm, as required to achieve ultra-high Q.

We fabricated our microresonators either from disk or cylinder blanks. The microresonators were first shaped by grinding or diamond-cutting tool and polished in an air-bearing spindle by successive smaller diamond particle slurries in order to obtain a smooth protrusion as visualized in Fig.1b. Their final diameters are $\sim 5 \text{ mm}$. We analyzed the microresonators in a scanning electron microscope. For instance we determined transverse radii of the crystalline MgF_2 disk of $\lesssim 50 \mu\text{m}$. The intensity profile of the fundamental WGM of the MgF_2 microresonator in the mid-IR is displayed in Fig.1(c). From finite element model simulations we obtained an effective mode area of $A_{\text{eff}} \sim 600 \mu\text{m}^2$ at $\lambda \sim 4.4 \mu\text{m}$. To ensure that we are not limited by scattering losses on residual surface roughness, their optical quality factors were first measured at $\lambda = 1.55 \mu\text{m}$ with a tunable, narrow-linewidth (short-term $< 100 \text{ kHz}$) fiber laser using silica tapered fibers to excite the WGM [30]. The MgF_2 disk features loaded optical factors of $Q \geq 5 \times 10^8$; CaF_2 and SrF_2 exhibit Q factors of $\sim 2 \times 10^9$ and the BaF_2 cylinder features $Q \sim 6.4 \times 10^9$ (detailed in a further section of the manuscript and in Figure 5).

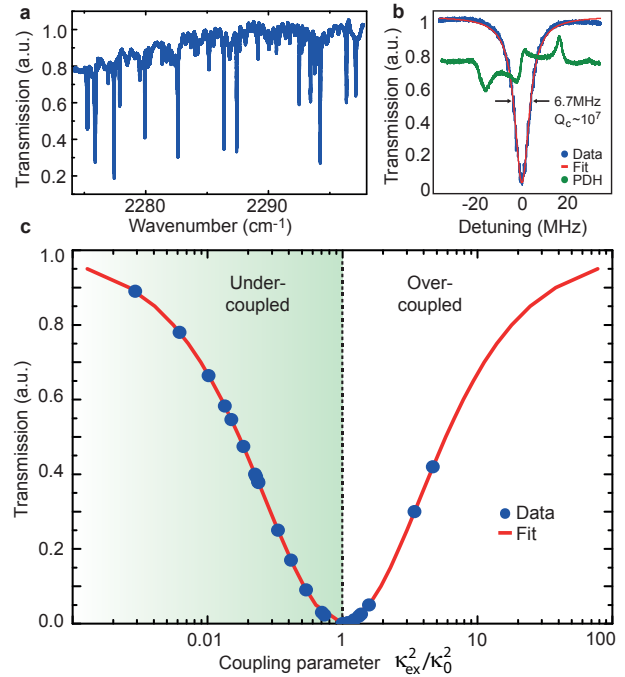


FIG. 2. **Characterization of taper-resonator coupling efficiency in the mid-IR spectral region around $4.5 \mu\text{m}$.** **a** Representative transmission spectrum composed of several resonance families over a wide mid-IR range when taper-resonator coupling is achieved. **b** Measurement of a resonance linewidth at critical coupling with frequency calibration provided by a Pound-Drever-Hall (PDH) signal (green curve) and Lorentzian fit (red curve). The typical FWHM width of $\kappa/2\pi \sim 6.7 \text{ MHz}$ corresponds to a critically coupled quality factor of $Q_c \sim 1.0 \times 10^7$. **c** Transmission as a function of the coupling parameter $\kappa_{\text{ex}}^2/\kappa_0^2$ for varying taper waist radius. The dashed line marks the critical coupling point ($\kappa_{\text{ex}} = \kappa_0$). The experimental data (blue circles) are consistent with the theoretical fit (red curve) demonstrating that the ChG taper behaves as a nearly ideal coupler in mid-IR with close to unity ideality.

III. UNCOATED CHALCOGENIDE TAPERED FIBERS AS HIGH IDEALITY MID IR COUPLERS

To measure far in the infrared, we used a mode-hop-free tunable QCL (Daylight Solutions Inc.). To couple QCL light into the microresonator we developed optical tapered fibers made out of ChG glass. ChG fibers are particularly attractive due to their low loss in the mid-IR [42] and commercial availability. However they were never used previously as a low loss, uncoated tapered optical waveguide because of technical fabrication challenges in their tapering process and maintenance, due to the low melting point of ChG glasses ($\sim 200^\circ\text{C}$ for As_2S_3). We have successfully developed a tapering setup with a feedback controlled electrical heater to adiabatically pull low loss uncoated tapered ChG fibers. To verify the theoretically expected taper waist, scanning

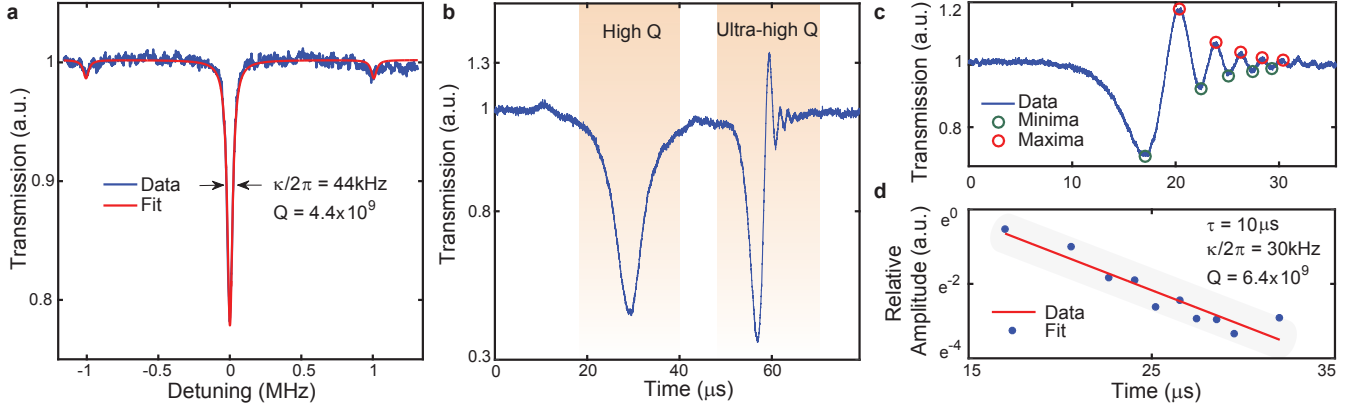


FIG. 3. Near-IR characterization of a BaF_2 microresonator. **a** Linewidth measurement of an under-coupled resonance with calibration sidebands (resulting from phase modulation of the laser) at 1 MHz and Lorentzian fit (red line). We extract a typical FWHM of $\kappa/2\pi \sim 44$ kHz resulting in an optical factor of $Q \sim 4.4 \times 10^9$. **b** Cavity-ringdown measurements. We observed the transmission spectrum of two resonances while scanning at the same speed. Only the ultra-high Q mode features a ringdown signal (right resonance). **c** Analysis of ringdown structure. We extract successive amplitudes of maxima (red circles) and of minima (green circles) to fit the evolution of the relative amplitude ringdown **d**. Theoretical fit of the ringdown relative amplitude (red line). The measured amplitude decay of $\tau = 10 \mu\text{s}$ results in a linewidth of $\kappa/2\pi = 30$ kHz and a Q factor of 6.4×10^9 .

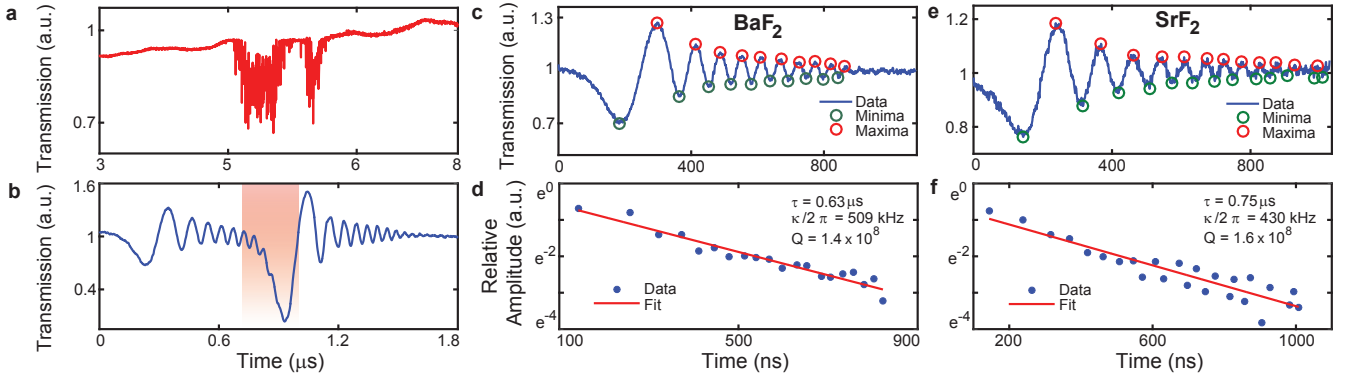


FIG. 4. Mid-IR swept frequency ringdown characterization of BaF_2 and SrF_2 microresonators. **a** Thermal distortions of a resonance in the BaF_2 crystalline microresonator. Thermal-optical dynamics prevent measuring the linewidth and the transmission accurately using standard frequency modulation spectroscopy method. **b** Using a cavity swept laser ringdown method, we observe modal coupling between two ultra-high Q resonances. **c,e** Transmission spectra of the ringdown signal of an ultra-high Q resonance in mid-IR at $4.4 \mu\text{m}$ using BaF_2 (c) and SrF_2 (e). **d,f** Exponential fits (red lines) of the measured data (blue circles) extracted from (c,e). In BaF_2 (d), the measured amplitude lifetime of $\tau = 0.63 \mu\text{s}$ results in a linewidth of $\kappa/2\pi = 509$ kHz and a corresponding Q factor of $\sim 1.4 \times 10^8$. In SrF_2 (f), the measured amplitude lifetime of $\tau = 0.75 \mu\text{s}$ results in a linewidth of $\kappa/2\pi = 430$ kHz and a corresponding Q factor of $\sim 1.6 \times 10^8$.

electron microscope images were taken to optimize the tapering process. The ChG (As_2S_3) tapered fiber was fabricated from a commercially available, IRflex IRF-S 10 nonlinear mid-IR fiber, made from extra high purity ChG glass. The fiber is transparent from 1.5 to $6.5 \mu\text{m}$ and has a core diameter of $10 \mu\text{m}$ and a high nonlinear refractive index of $n_2 = 2.7$. The ChG tapered fiber was pulled down to a diameter to phase match the fundamental WGM. For instance, for a MgF_2 microresonator radius of $R \sim 2.5$ mm, the optimum taper waist in the mid-IR corresponds to a subwavelength diameter of $1.2 \mu\text{m}$ (Fig.1(d)). The experimental setup is described in

Fig.1e. The pump laser is a 200 mW continuous wave QCL external cavity laser, tunable from 4.385 to $4.58 \mu\text{m}$. Tapered fiber and microresonator are kept under a dry and inert atmosphere to preserve from degradation. The QCL light is evanescently coupled to the crystalline microresonator using the ChG tapered fiber. When the taper-resonator coupling is achieved, several resonance families are observed at $\lambda \sim 4.4 \mu\text{m}$, as illustrated in Fig.2(a).

A unique property of taper-coupled microresonators is that phase matching (and thus the coupling) can be finely tuned by translating the microresonator along the taper

relative to the waist [37]. We investigated in detail the mid-IR coupling behavior between the ChG taper and the MgF_2 crystalline microresonator for a typical mode family. For an unity ideality coupler [38], the coupling parameter is given by $\kappa_{\text{ex}}^2/\kappa_0^2 = (1 \pm \sqrt{T})/(1 \mp \sqrt{T})$, where κ_0 is the intrinsic loss rate, κ_{ex} the photon loss rate due to coupling to the microresonator and T the transmission on resonance. The upper signs are used for transmission values T in the over-coupled regime ($\kappa_0 < \kappa_{\text{ex}}$) and the lower signs for the under-coupled regime ($\kappa_0 > \kappa_{\text{ex}}$). We recorded the transmission spectrum while scanning the laser over resonance for different taper waist radii. We measured the corresponding full-width at half maximum (FWHM) linewidth by setting up a Pound-Drever-Hall (PDH) technique with a mid-IR electro-optic phase modulator (Qubig GmbH) to provide frequency calibration. Figure 2(c) shows the normalized transmission as a function of the parameter $\kappa_{\text{ext}}^2/\kappa_0^2$. Critical ($\kappa_0 = \kappa_{\text{ex}}$) and strong overcoupling up to $\kappa_{\text{ex}}/\kappa_0 \sim 6$ are observed for optimum taper diameters. We emphasize that this represents the first achievement of critical coupling in crystalline microresonators in the mid-IR region. This reveals that the ChG taper behaves as a nearly ideal coupler, with close to unity ideality [38]. We measured a linewidth of $\kappa/2\pi \sim 6.7$ MHz at critical coupling (red curve in Fig.2b.) yielding an optical factor of $Q_c \sim 1.01 \times 10^7$ for MgF_2 . Our measurements reveal that uncoated ChG tapers can thus extend the efficient tapered fiber coupling method deep to the mid-IR regime. It enables a complete characterization control and use of microresonators in the mid-IR, in contrast to other methods such as prism coupling [35, 36].

IV. NEAR- AND MID-IR CAVITY RINGDOWN MEASUREMENTS OF CRYSTALLINE MICRORESONATORS

After MgF_2 characterization, we studied other fluoride crystals employed in this work (CaF_2 , BaF_2 , SrF_2) and first characterized them in the near-IR setup. We measured the optical Q factor using both linewidth calibration and a swept laser cavity ringdown technique. The cavity ringdown method enables a measurement of the quality factor independently of the thermal nonlinearity (hence at higher pumping powers) and of the laser linewidth. Fig.4(a) shows a typical resonance obtained in the under-coupled regime for a pump power of $P \leq 1$ mW in BaF_2 . The Lorentzian fit gives a FWHM linewidth of $\kappa/2\pi \sim 44$ kHz at 1555 nm, resulting in an optical factor of $Q \sim 4.4 \times 10^9$. From the coupling curve we can extract moreover an intrinsic linewidth of $\kappa_0/2\pi \sim 22$ kHz (corresponding to an intrinsic Q of 0.9×10^{10}). In addition, we performed swept laser cavity ringdown measurements [30] to first calibrate the method in the near-IR. When an ultra-high Q resonator is excited with a laser whose frequency is linearly swept across the resonance with a duration shorter than the cavity lifetime, its transmission

spectrum shows oscillations (see Fig.4.(b)). These oscillations result from the beating of the transiently build-up light inside the resonator that decays into the fiber, with that of the swept laser source. Importantly, when the laser is swept fast, the two components will have a different beat frequency giving rise to an exponentially decaying oscillation. In the case of a lower Q mode (with negligible cavity buildup), no ringdown signal is observed at the same scan speed, as highlighted in Fig.4.(b). We analyzed the transmission spectrum of the ringdown structure in Fig.4.(c) by measuring the amplitude decay τ of the remitted light [28]. Its theoretical fit (Fig.4(d)) gives a measured amplitude decay τ of 10 μs , corresponding to an intrinsic cavity Q_0 of $\sim 6.4 \times 10^9$. This value is close to the one derived with the frequency modulation spectroscopy, corroborating the faithfulness of the method. In CaF_2 and SrF_2 microresonators we measured $\tau \sim 3$ μs , corresponding to an intrinsic cavity $Q_0 \sim 1.8 \times 10^9$, in agreement with the values derived from frequency modulation spectroscopy. We precise that we did not resort to annealing and/or baking procedures to improve Q factors of our microresonators [28].

Having established the ultra-high Q resonance in the near-IR, and having developed the mid-IR ChG tapered fiber method, we afterwards measured Q factors in the mid-IR. Phase matching between the ChG tapered fiber and the microresonator is achieved by translating the taper position. In contrast to the near-IR, when coupling is achieved, we observed large thermal instability in the mid-IR [43]. These thermal instabilities induce large distortions of the resonance (see Fig.4.(a)) preventing any reliable measurement of its linewidth using the PDH error signal as a calibration. In that case, the optical Q factor can only be inferred by cavity ringdown measurements. We scanned the QCL using its laser current modulation in order to observe the cavity ringdown signal. Amplitude and cavity lifetime depend on coupling and linewidth of the resonance. When two resonances are really close, we observe a modal coupling between the two oscillatory decaying signals (see Fig.4.(b)) [44]. The BaF_2 transmission spectrum of a typical ringdown structure is displayed in Fig.4.(c). By measuring the amplitude decay τ of the remitted light (Fig.4(d)), we obtained a BaF_2 intrinsic factor of $Q_0 = \omega\tau/2 \sim 1.4 \times 10^8$.

TABLE I. Experimentally measured mid-IR absorption properties of different crystalline fluoride materials, at 4.4 μm

Crystal	$\kappa/2\pi$	Q_0	α (cm^{-1})	\mathcal{F}
MgF_2	3.4 MHz	2×10^7	9×10^{-4}	4×10^3
CaF_2	710 kHz	9.6×10^7	2×10^{-4}	2×10^4
BaF_2	509 kHz	1.4×10^8	1.4×10^{-4}	3×10^4
SrF_2	430 kHz	1.6×10^8	1.2×10^{-4}	4×10^4

CaF_2 and SrF_2 crystals were studied by applying the same methods. The ringdown analysis in the case of SrF_2 is presented in Fig.4(e). We measured an amplitude de-

cay time τ of $0.75 \mu\text{s}$ (Fig.4(f)), resulting in an intrinsic factor of $Q_0 = \omega\tau/2 \sim 1.6 \times 10^8$. We precise that no ringdown was observed when measuring the Q factor of the MgF_2 microresonator under the same conditions, confirming that MgF_2 does not feature ultra-high Q factors in the mid-IR [36]. Table I and Fig.5 summarize the results of our measurements. From these measurements we extracted the limiting values of the mid-IR intrinsic absorption $\alpha \leq \frac{2\pi n}{Q\lambda}$ at $4.4 \mu\text{m}$. We show that the absorption can thus be as low as 100 ppm/cm for SrF_2 . Translated to a single round-trip in a Fabry-Pérot cavity of length $L/2$ (where $L = 2\pi r$ for a WGM of radius r) and finesse \mathcal{F} , this value amounts to optical losses (absorbance) of the order of $\alpha L = \frac{2\pi}{\mathcal{F}}$, i.e. 150 ppm.

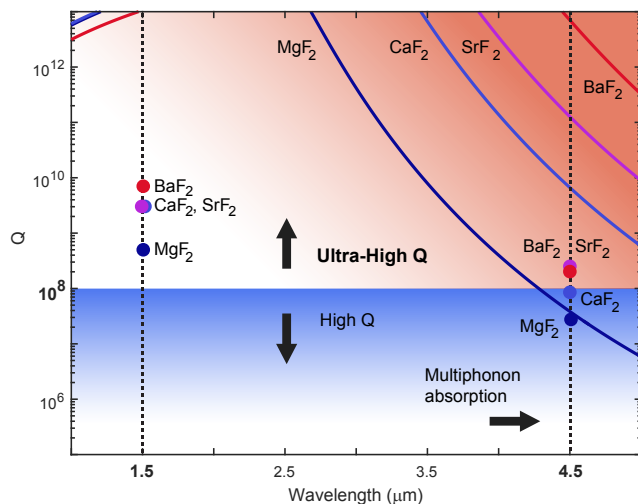


FIG. 5. **Mid-IR ultra-high Q microcavities based on alkaline earth metal fluoride crystalline materials.** Measurements for different fluoride crystals of the XF_2 family (where $X = \text{Ca}, \text{Mg}, \text{Ba}, \text{Sr}$) prove the possibility of attaining the ultra-high Q regime in the mid-IR. Except for MgF_2 , for which we reach the theoretical limit imposed by multiphonon absorption at room temperature, other materials offer $Q \geq 10^8$ around $4.5 \mu\text{m}$. The lines represent the theoretical multiphonon absorption limit of Q with respect to the wavelength. The circles represent our experimental values. Despite the clear differences with the near-IR region, mid-IR cavities are able to overcome the high- Q regime achieving $Q > 10^8$.

V. CONCLUSIONS

In summary, we have demonstrated for the first time mid-IR ultra-high Q crystalline resonators made from

commercially available BaF_2 and SrF_2 crystals at $4.5 \mu\text{m}$, a region of high interest due to the transparency of the atmosphere and absorption of toxic or greenhouse molecules (e.g. CO , CO_2 , SO_2 or CO_3) and the availability of QCL laser sources. Moreover we show that MgF_2 crystals operate close to the fundamental limit imposed by multiphoton absorption in the mid-IR. We show that uncoated chalcogenide tapered fibers can be ideal and efficient couplers deep to the mid-IR. Together with cavity ringdown methods, our platform enables precise measurements of quality factor, overcoming previous limitations. We show that a finesse as high as $\mathcal{F} \sim 4 \times 10^4$ is achievable with BaF_2 and SrF_2 in the mid-IR for cavities as small as few millimeters in diameter. This finesse represents a more than 1 order of magnitude improvement over prior high finesse cavities in this wavelength range [8–10]. Our results in the mid-IR pave the way to the next generation of ultra-stable sources and ultra-precise spectrometers in the molecular fingerprint region and can further leverage QCL technology, by e.g. enabling injection locked QCL similar to technology developed in the near-IR [16, 34]. Despite the differences with near-IR, we prove that the mid-IR region is not limited to the high- Q regime when proper materials are used. The materials crystalline nature leads to low thermodynamical noise [26] and moderate multiphonon absorption in the highly-relevant mid-IR region. In addition, combining QCL with mid-IR ultra-high Q crystalline microresonators opens a route for mid-IR Kerr comb or soliton generation [33, 45, 46].

FUNDING INFORMATION

This work was gratefully supported by the Defense Advanced Research Program Agency (DARPA) under the PULSE program and by grant N° IZLRZ2_163864 from the Swiss National Science Foundation (SNSF). C. L. gratefully acknowledges support from the European Commission through Marie Skłodowska-Curie Fellowships: IEF project 629649.

ACKNOWLEDGMENTS

We gratefully acknowledge helpful discussions with Yanne Chembo. We acknowledge technical support from Arnaud Magrez, Qubig GmbH and IRflex Corporation.

[1] Lines, M. E. Ultralow-loss glasses. *Annual Review of Materials Science* **16**, 113–135 (1986).

[2] Thorpe, M. J. Broadband Cavity Ringdown Spectroscopy for Sensitive and Rapid Molecular Detection.

- Science* **311**, 1595–1599 (2006).
- [3] Coddington, I., Swann, W. C. & Newbury, N. R. Coherent multiheterodyne spectroscopy using stabilized optical frequency combs. *Physical Review Letters* **100**, 013902 (2008).
 - [4] Thorpe, M. J. *et al.* Cavity-enhanced optical frequency comb spectroscopy: application to human breath analysis. *Optics Express* **16**, 2387–97 (2008). 0706.1582.
 - [5] Paul, J. B., Lapson, L. & Anderson, J. G. Ultrasensitive absorption spectroscopy with a high-finesse optical cavity and off-axis alignment. *Applied optics* **40**, 4904–4910 (2001).
 - [6] Brown, S. Absorption spectroscopy in high finesse cavities for atmospheric studies. *Chemical Reviews* **103**, 5219 (2003).
 - [7] Savchenkov, A. A. *et al.* Low threshold optical oscillations in a whispering gallery mode CaF_2 resonator. *Physical Review Letters* **93**, 243905 (2004).
 - [8] Schwarzl, T. *et al.* Mid-infrared high finesse microcavities and vertical-cavity lasers based on IV–VI semiconductor/BaF₂ broadband Bragg mirrors. *Journal of Applied Physics* **101** (2007).
 - [9] Alligood Deprince, B., Rocher, B. E., Carroll, A. M. & Widicus Weaver, S. L. Extending high-finesse cavity techniques to the far-infrared. *Review of Scientific Instruments* **84** (2013).
 - [10] Foltynowicz, A., Maslowski, P., Fleisher, A. J., Bjork, B. J. & Ye, J. Cavity-enhanced optical frequency comb spectroscopy in the mid-infrared application to trace detection of hydrogen peroxide. *Applied Physics B: Lasers and Optics* **110**, 163–175 (2013). 1202.1216.
 - [11] Siciliani de Cumis, M. *et al.* Microcavity-Stabilized Quantum Cascade Laser. *Laser & Photonics Reviews* **10**, 153–157 (2016).
 - [12] Faist, J. *et al.* Quantum Cascade Laser. *Science* **264**, 553–556 (1994).
 - [13] Yao, Y., Hoffman, A. J. & Gmachl, C. F. Mid-infrared quantum cascade lasers. *Nature Photonics* **6**, 432–439 (2012).
 - [14] Argence, B. *et al.* Quantum cascade laser frequency stabilization at the sub-Hz level. *Nature Photonics* **9**, 456–460 (2015).
 - [15] Kessler, T. *et al.* A sub-40-mHz-linewidth laser based on a silicon single-crystal optical cavity. *Nature Photonics* **6**, 687–692 (2012). 1112.3854.
 - [16] Liang, W. *et al.* Ultralow noise miniature external cavity semiconductor laser. *Nature Communications* **6**, 7371 (2015).
 - [17] Vollmer, F. & Arnold, S. Whispering-gallery-mode biosensing : label-free detection down to single molecules. *Nature Methods* **5**, 591–596 (2008).
 - [18] Orr, B. J. & He, Y. Rapidly swept continuous-wave cavity-ringdown spectroscopy. *Chemical Physics Letters* **512**, 1–20 (2011).
 - [19] Kippenberg, T. J., Holzwarth, R. & Diddams, S. A. Microresonator-Based Optical Frequency Combs. *Science* **332**, 555–559 (2011).
 - [20] Way, B., Jain, R. K. & Hossein-Zadeh, M. High-Q microresonators for mid-IR light sources and molecular sensors. *Optics letters* **37**, 4389–91 (2012).
 - [21] Ma, P. *et al.* High Q factor chalcogenide ring resonators for cavity-enhanced MIR spectroscopic sensing. *Optics Express* **23**, 19969 (2015).
 - [22] Singh, V. *et al.* Mid-infrared materials and devices on a Si platform for optical sensing. *Science and Technology of Advanced Materials* **15**, 014603 (2014).
 - [23] Shankar, R., Bulu, I. & Lončar, M. Integrated high-quality factor silicon-on-sapphire ring resonators for the mid-infrared. *Applied Physics Letters* **102**, 051108 (2013).
 - [24] Lin, H. *et al.* Demonstration of high-Q mid-infrared chalcogenide glass-on-silicon resonators. *Optics Letters* **38**, 1470–1472 (2013).
 - [25] Chen, Y., Lin, H., Hu, J. & Li, M. Heterogeneously integrated silicon photonics for the mid-infrared and spectroscopic sensing. *ACS Nano* **8**, 6955–6961 (2014).
 - [26] Cole, G. D., Zhang, W., Martin, M. J., Ye, J. & Aspelmeyer, M. Tenfold reduction of Brownian noise in high-reflectivity optical coatings. *Nature Photonics* **7**, 644–650 (2013). 1302.6489.
 - [27] Cole, G. Crystalline mirrors solutions gmbh. (private communication).
 - [28] Savchenkov, A. A., Matsko, A. B., Ilchenko, V. S. & Maleki, L. Optical resonators with ten million finesse. *Optics Express* **15**, 6768 (2007).
 - [29] Grudinin, I. S., Ilchenko, V. S. & Maleki, L. Ultrahigh optical Q factors of crystalline resonators in the linear regime. *Physical Review A* **74**, 1–9 (2006).
 - [30] Hofer, J., Schliesser, A. & Kippenberg, T. J. Cavity optomechanics with ultrahigh-Q crystalline microresonators. *Physical Review A* **82** (2010).
 - [31] Lin, G., Diallo, S., Henriët, R., Jacquot, M. & Chembo, Y. K. Barium fluoride whispering-gallery-mode disk-resonator with one billion quality-factor. *Optics Letters* **39**, 6009–6012 (2014).
 - [32] Henriët, R. *et al.* Kerr optical frequency comb generation in strontium fluoride whispering-gallery mode resonators with billion quality factor. *Optics Letters* **40**, 1567–1570 (2015).
 - [33] Herr, T. *et al.* Temporal solitons in optical microresonators. *Nature Photonics* **8**, 145–152 (2013).
 - [34] Liang, W. *et al.* High spectral purity Kerr frequency comb radio frequency photonic oscillator. *Nature communications* **6**, 7957 (2015).
 - [35] Savchenkov, A. A. *et al.* Generation of kerr combs centered at 4.5 μm in crystalline microresonators pumped with quantum-cascade lasers. *Optics Letters* **40**, 3468–3471 (2015).
 - [36] Grudinin, I. S., Mansour, K. & Yu, N. Fluoride microresonators for mid-IR applications. *ArXiv e-prints* (2016). 1602.00736.
 - [37] Cai, M., Painter, O. & Vahala, K. J. Observation of critical coupling in a fiber taper to a silica-microsphere whispering-gallery mode system. *Physical Review Letters* **85**, 74–77 (2000).
 - [38] Spillane, S., Kippenberg, T., Painter, O. & Vahala, K. Ideality in a fiber-taper-coupled microresonator system for application to cavity quantum electrodynamics. *Physical Review Letters* **91**, 043902 (2003).
 - [39] Hass, M. & Bendow, B. Residual absorption in infrared materials. *Applied optics* **16**, 2882–2890 (1977).
 - [40] Bendow, B., Lipson, H. G. & Mitra, S. S. Multiphonon infrared absorption in highly transparent MgF_2 . *Physical Review B* **20**, 1747–1749 (1979).
 - [41] Gorodetsky, M. L., Savchenkov, A. A. & Ilchenko, V. S. Ultimate Q of optical microsphere resonators. *Optics letters* **21**, 453–455 (1996).

- [42] Eggleton, B. J., Luther-Davies, B. & Richardson, K. Chalcogenide photonics. *Nature Photonics* **5**, 141–148 (2011).
- [43] Fomin, A. E., Gorodetsky, M. L., Grudinin, I. S. & Ilchenko, V. S. Nonstationary nonlinear effects in optical microspheres. *Journal of the Optical Society of America B* **22**, 459 (2005).
- [44] Trebaol, S., Dumeige, Y. & Féron, P. Ringing phenomenon in coupled cavities: Application to modal coupling in whispering-gallery-mode resonators. *Physical Review A* **81** (2010).
- [45] Yi, X., Yang, Q.-F., Yang, K. Y., Suh, M.-G. & Vahala, K. Soliton frequency comb at microwave rates in a high-Q silica microresonator. *Optica* **2**, 1078 (2015).
- [46] Brasch, V. *et al.* Photonic chip-based optical frequency comb using soliton cherenkov radiation. *Science* **351**, 357–360 (2016).